

1 **Experimental evaluation of the dosimetric impact of intrafraction prostate**
2 **rotation using film measurement with a 6DoF robotic arm**

3 Kehuan Shi¹, Andrew Dipuglia², Jeremy Booth², Saree Alnaghy³, Andre Kyme⁴, Paul Keall¹
4 and Doan Trang Nguyen^{1,5}

5 1. ACRF Image-X Institute, Central Clinical School, University of Sydney, Sydney, NSW,
6 Australia

7 2. Northern Sydney Cancer Centre, Royal North Shore Hospital, St Leonards, NSW,
8 Australia

9 3. Centre for Medical Radiation Physics, University of Wollongong, Wollongong, NSW,
10 Australia

11 4. School of Biomedical Engineering, University of Sydney, Sydney, NSW, Australia

12 5. School of Biomedical Engineering, University of Technology Sydney, Sydney, NSW,
13 Australia

14 Correspondence: DoanTrang.Nguyen@uts.edu.au

15

16

17

Abstract

18 **Purpose:**

19 Tumor motion during radiotherapy can cause a reduction in target dose coverage and an
20 increase in healthy tissue exposure. Tumor motion is not strictly translational and often
21 exhibits complex six degree-of-freedom (6DoF) translational and rotational motion. Although
22 the dosimetric impact of prostate tumor translational motion is well investigated, the
23 dosimetric impact of 6DoF motion has only been studied with simulations or dose
24 reconstruction. The present study aims to experimentally quantify the dose error caused by
25 6DoF motion. The experiment was designed to test the hypothesis that 6DoF motion would
26 cause larger dose errors than translational motion alone through gamma analyses of 2D film
27 measurements.

28 **Methods:**

29 Four patient-measured intrafraction prostate motion traces and four VMAT 7.25Gy/Fx SBRT
30 treatment plans were selected for the experiment. The traces represented typical motion
31 patterns, including small-angle rotations ($<4^\circ$), transient movement, persistent excursion and
32 erratic rotations ($>6^\circ$). Gafchromic film was placed inside a custom-designed phantom, held
33 by a high precision 6DoF robotic arm for dose measurements in the coronal plane during
34 treatment delivery. For each combination of the motion trace and treatment plan, two film
35 measurements were made, one with 6DoF motion and the other with the 3D translation
36 components of the same trace. A gamma pass rate criteria of 2% relative dose/2 mm
37 distance-to-agreement was used in this study and evaluated for each measurement with
38 respect to the static reference film. Two test thresholds, 90% and 50% of the reference dose,
39 were applied to investigate the difference in dose coverage for the PTV region and
40 surrounding areas, respectively. The hypothesis was tested using a Wilcoxon signed-rank
41 test.

42 **Results:**

43 For each of the sixteen plan and motion trace pairs, a reduction of the gamma pass rate was
44 observed for 6DoF motion compared with 3D translational motion. With 90% gamma-test
45 threshold, the reduction was $5.8\% \pm 7.1\%$ ($p < 0.01$). With 50% gamma-test threshold, the
46 reduction was $4.1\% \pm 4.8\%$ ($p < 0.01$).

47 **Conclusion:**

48 For the first time, the dosimetric impact of intrafraction prostate rotation during SBRT
49 treatment was measured experimentally. The experimental results support the hypothesis
50 that 6DoF tumor motion causes higher dose error than translation motion alone.

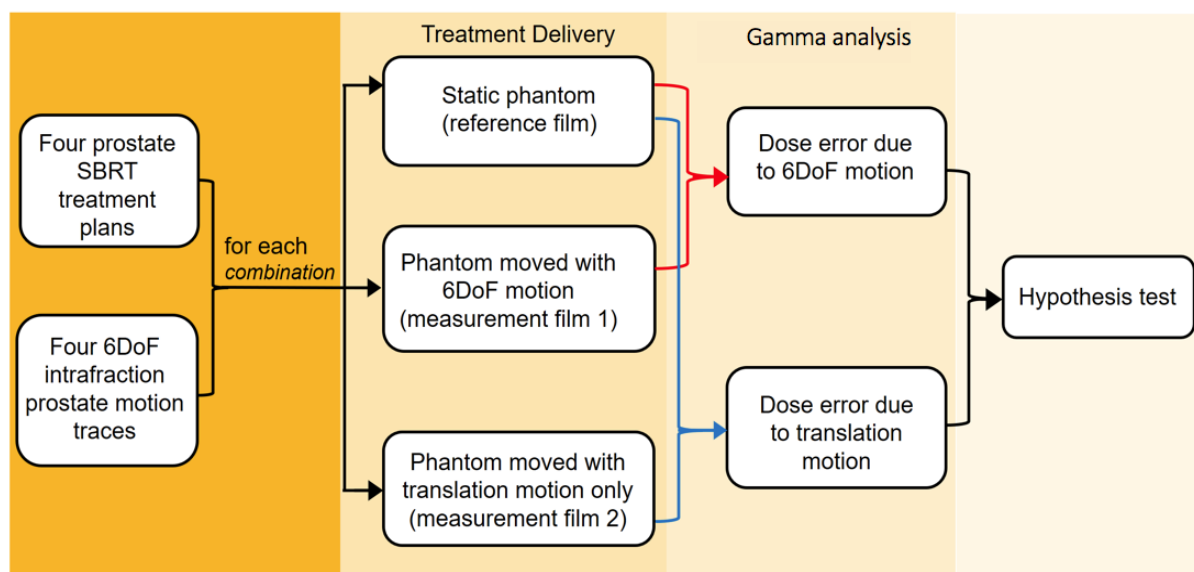
51 1. Introduction

52 The range and distribution of intrafraction prostate motion observed in patients has been
53 reported in a number of studies.^[1-3] An analysis of prostate intrafraction translational motion
54 in 427 patients found that displacement >2mm occurred in 66% of fractions while 28% of
55 fractions had >3mm displacement.^[4] In addition to translational motion, the prostate motion
56 also includes rotation. Prostate intrafraction rotations were reported to be small in most
57 cases.^[5-7] The most dominant rotations were observed to be around the left-right (LR) axis.^[1,8]
58 Intrafraction rotations of $2.5^{\circ}(\pm 2.3^{\circ})$ around the LR axis were reported in a study on 39
59 prostate cancer patients.^[3] However, in extreme cases, the rotational motion can reach
60 beyond 10° .^[6,8]

61 Simulation studies suggest that the dosimetric effect of prostate intrafraction
62 rotational motion is significant. A simulation study on 548 prostate motion trajectories^[9]
63 showed that rotational corrections up to 5° were required to achieve 98% Clinical Target
64 Volume (CTV) coverage in 98% of the treatments. In addition, it was found that a 3 mm CTV
65 to Planning Target Volume (PTV) margin was only sufficient for adequate CTV D_{95} coverage
66 in 65% of the 26 patients.^[6] Rijkhorst et al ^[10] suggested an additional 4 mm margin was
67 needed to account for tumor rotation.

68 To date, the dosimetric effect of intrafraction prostate rotation was studied only
69 through simulation or retrospective dose reconstruction. The majority of studies used
70 averaged rotation displacement to quantify the effect of intrafraction rotation. In this paper,
71 we describe an experimental evaluation of the dosimetric impact of intrafraction 6DoF motion
72 on prostate SBRT treatment. The experiment was designed to test the hypothesis that
73 intrafraction 6DoF motion would cause a larger dosimetric error compared with translational
74 motion only, and to quantify the magnitude of this difference.

75 2. Materials and Methods

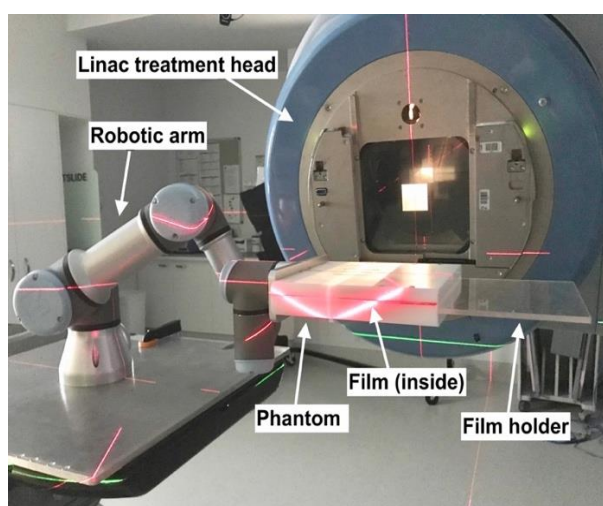


76
77

Figure 1: Process chart for the experiment.

78 2.1 Experimental Setup

79 The experiment was designed to measure coronal plane dose distributions of prostate SBRT
80 treatment plans using film. The phantom holding the film was positioned at isocenter and
81 moved by a programmable robotic arm according to measured patient 6DoF motion
82 trajectories. The experimental process is illustrated in Figure 1 and the experimental setup is
83 shown in Figure 2.



84
85

Figure 2: The experimental setup: a plastic phantom containing film was attached to a programmable 6DoF robot. The robot was used to replicate patient-measured prostate motion during treatment delivery.

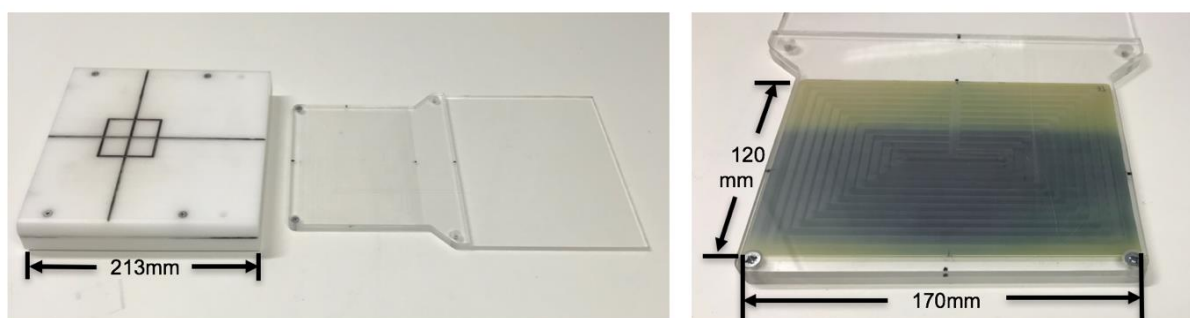
87

88 2.2 6DoF robotic arm

89 A programmable 6DoF robotic arm (UR3 robot, Universal Robots, Odense Denmark) was
 90 chosen for its wide range of movement and high localization accuracy. The six rotating joints,
 91 each with a 360° range, and 500 mm reach enable the robot to reproduce translational or
 92 rotational organ movement.^a In-house software was used to interface with the robot. The
 93 dynamic localization accuracy of the robotic arm in reproducing motion traces is <0.2 mm
 94 and $<0.2^\circ$ for translation and rotation, respectively.^[11]

95 **2.3 Phantom and film**

96 The phantom was made of polyoxymethylene acetal (density= 1.4 g/cm³) with outer
 97 dimensions $213 \times 200 \times 40$ mm³. Its inner structure was an exact fit to the transparent film
 98 holder to allow easy slide-in and fixation. The film holder comprised a two-layer structure
 99 made of Polymethyl methacrylate (PMMA, density= 1.16 g/cm³) with a thin layer of hollow
 100 space (120×170 mm²) for the film to fit (Figure 3).



101
 102 Figure 3: Left, custom-designed polyoxymethylene phantom and plastic PMMA film holder.
 103 Right, post-irradiation film inside the film holder.

104
 105 The film used in the experiment was Gafchromic™ EBT3 dosimetry film (Ashland Advanced
 106 Materials, New York, USA). The EBT3 film was selected as the dosimeter for these
 107 experiments as it has a surface spatial resolution of ≤ 25 μ m and a dynamic range of 0.1 Gy
 108 to 20 Gy.^b

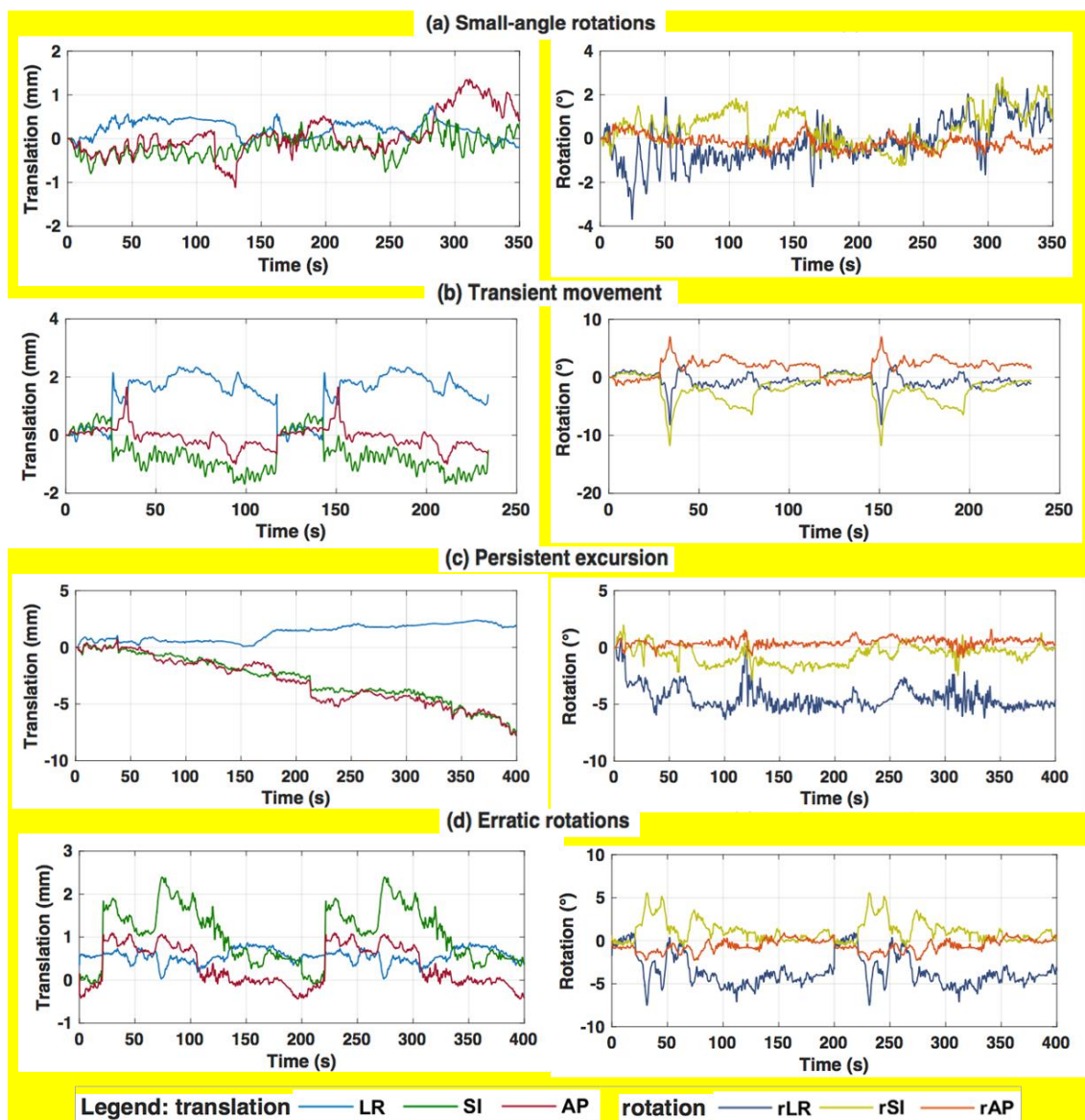
109 **2.4 Motion traces**

110 The motion traces (Figure 4) used in the experiment were acquired during SBRT treatments
 111 of prostate cancer patients enrolled in the TROG15.01 SPARK (Stereotactic Prostate
 112 Adaptive Radiotherapy utilizing Kilovoltage Intrafraction Monitoring) trial.^[12] The motion
 113 monitoring method, Kilovoltage Intrafraction Monitoring (KIM), reconstructed the real-time 3D

114 positions of gold fiducial markers inside the prostate based on their 2D X-ray projections,¹³
115 and then computed 6DoF translation and rotation around the center-of-mass of the fiducial
116 markers using an iterative closest point (ICP) algorithm.^[7,14] Four traces representing four
117 typical types of observed prostate intrafraction rotation were selected.

118 As shown in Figure 4, the first trace (Figure 4.a) consisted of continuous small-angle (<4°)
119 rotations around all three axes, which represented the most prevalent pattern found in
120 published studies: a mean motion magnitude below 3°. ^[3,5,7,15] The second trace (Figure 4.b)
121 included a transient large-angle deflection that went beyond 10°, an example of extreme
122 motion.^[6,8] In the third trace (Figure 4.c), there was a persistent rotational excursion (average
123 4.5°) about the LR axis while the rotation about the other two axes was small, corresponding
124 to the dominance of rotations about the LR axis in most patients.^[1,8] In all but the third trace,
125 the translation motion was small (<3 mm). In the third trace, the translation motion exhibited
126 a slow drift pattern in the SI and AP direction. The fourth trace (Figure 4.d) was selected to
127 study the impact of large-angle (>6°) and high-frequency erratic behaviors of tumor rotation.

128 As the experiment delivery duration exceeded the duration of the second and fourth traces,
129 these traces were repeated. A low-pass filter was applied to each trace to eliminate
130 measurement noise.



131

132

133

134

135

2.5 Treatment plans

136

137

138

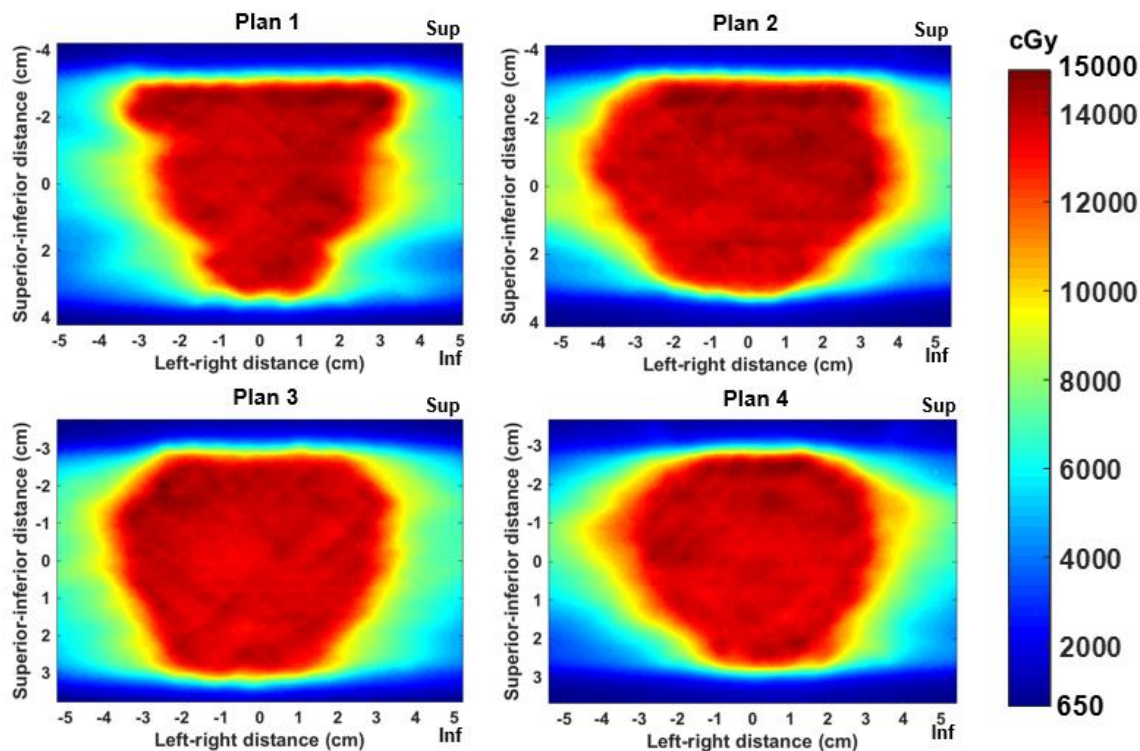
139

140

141

Figure 4: The four selected clinical prostate motion traces used in the study. Plots show translation (mm) in the left-right (LR), superior-inferior (SI) and anterior-posterior (AP) directions and rotation (degrees) about the three corresponding axes (rLR, rSI and rAP).

Four VMAT 6MV treatment plans, designed to deliver 7.25Gy per fractions in two arcs (240° to 120° and 120° to 240°), from the SPARK trial were used for investigation in the experiment. Details on the planning constraints can be found in Keall et. al (2015).¹⁶ The PTV cross-section of the plans differed in shape, ranging from relatively circular to wedge-shaped, as can be seen in the dose distributions of the reference film measurement for each plan (Figure 5).



142

143 Figure 5: Measured coronal reference dose distributions for the four prostate SBRT

144 treatment plans. There was no phantom motion for these reference scans.

145

146 For each treatment plan, one static coronal film measurement of the dose delivery at

147 isocenter was obtained first to serve as the reference film. After that, for each motion trace,

148 two film measurements were made while the robot replicated full 6DoF motion and 3D

149 translation only, respectively.

150 **2.6 Film processing**

151 All the film pieces were scanned at 75 dpi by a 48-bit flatbed RGB color scanner (EPSON

152 Expression 12000XL, Seiko Epson Corporation, Nagano, Japan). Each piece of

153 measurement film was scanned before and after radiation exposure to calculate the net

154 change in optical density (OD) with 2D uniformity correction applied using DoseLab (version

155 6.80, Varian Medical System). The net OD was converted to dose with accuracy of 0.1 cGy,

156 following AAPM TG-69.^[17]

157 Each measurement film was registered to the reference film manually. Following film
158 registration, a gamma test^[18] using a criteria of 2% relative dose/2 mm distance-to-
159 agreement (DTA) between the measured film and the reference film was performed. The test
160 criteria were stricter than 3%/3 mm as suggested for IMRT commissioning in AAPM TG-
161 119^[19]. The reference dose in each test was the D_{max} of the reference (static measurement).
162 Two test thresholds, 90% and 50% of the reference dose, were applied to investigate the
163 difference in dose coverage for the PTV region and surrounding areas, respectively.
164 To evaluate whether the pass rate difference was statistically significant, a Wilcoxon signed-
165 rank test was performed on the two groups of gamma pass rate data for 6DoF motion and
166 3D translation. This test was chosen based on the small sample size and the unknown
167 population distribution.

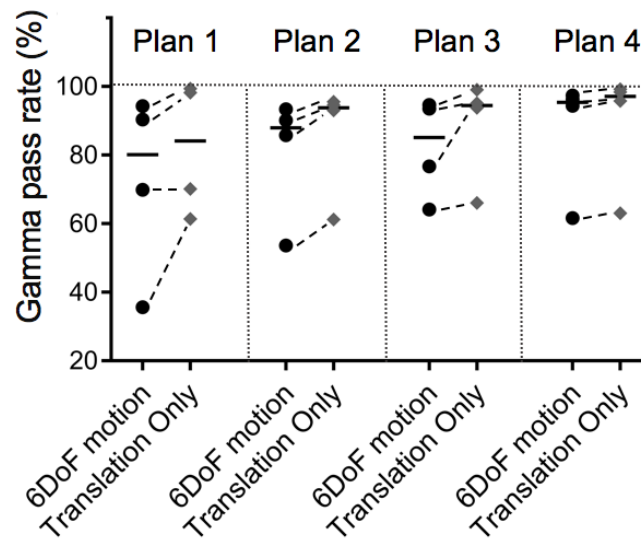
168

169 **3. Results**

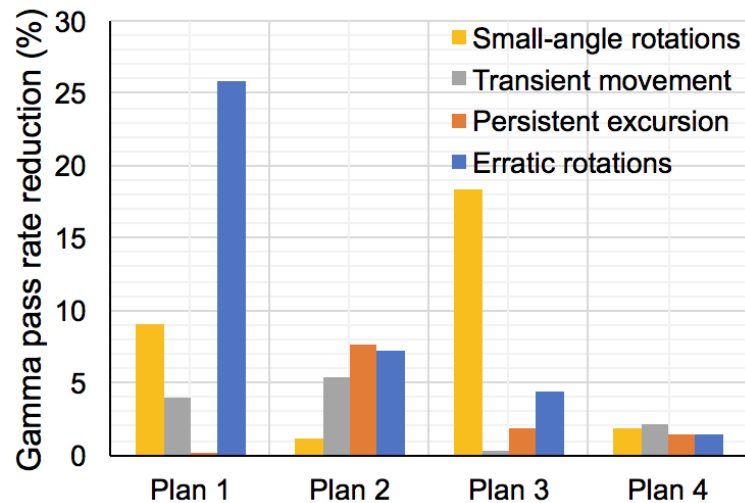
170 A summary of the gamma pass rates with 90% test threshold is plotted in Figure 6 (top).
171 Including rotation caused a reduction of the gamma pass rate in all cases compared with
172 translation alone (Figure 6, bottom). The mean reduction was 5.8% with a standard deviation
173 of 7.1% (range: [0.2%, 25.8%]). The reduction in gamma pass rates in the film's PTV region
174 due to added rotation was statistically significant ($p < 0.01$).

175

Summary of gamma pass rates with different traces
test threshold = 90%



Gamma pass rate reduction due to rotation
test threshold = 90%



176

177

178 Figure 6: Gamma pass rate data for a 90% test threshold of the reference dose. Top,

179 summary of the gamma pass rates for each plan, with a dashed line connecting trace pair

180 results and the median bar for results from the same trace. Bottom, summary of the

181 reduction in pass rates caused by rotation for **each tested prostate trace.**

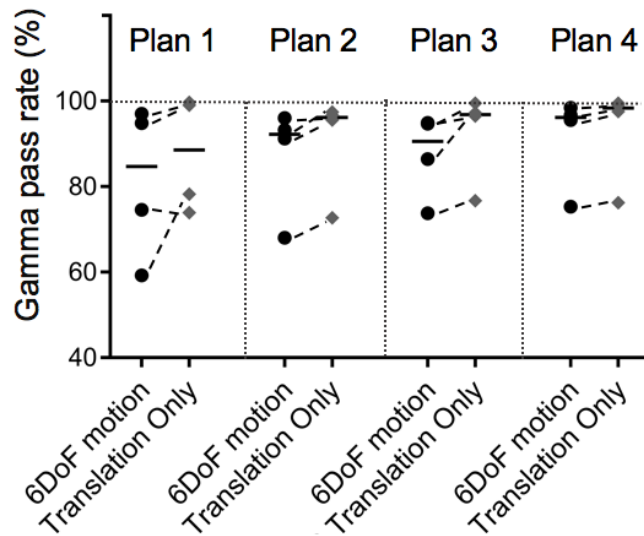
182

183 Results for a test threshold of 50% of the PTV dose are summarized in Figure 7. In this case

184 the mean gamma pass rate reduction due to rotation was 4.1% with a standard deviation of

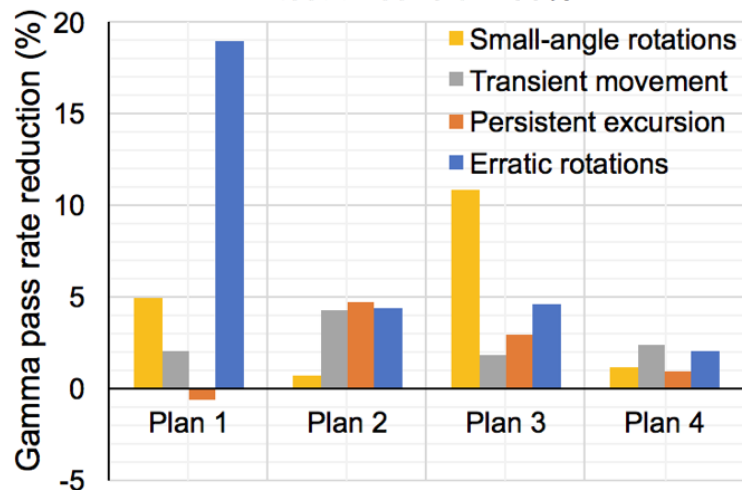
185 4.8% (range: [-0.7%, 19%]). The reduction was also statistically significant ($p < 0.01$).

Summary of gamma pass rates with different traces
test threshold = 50%



186

Gamma pass rate reduction due to rotation
test threshold = 50%



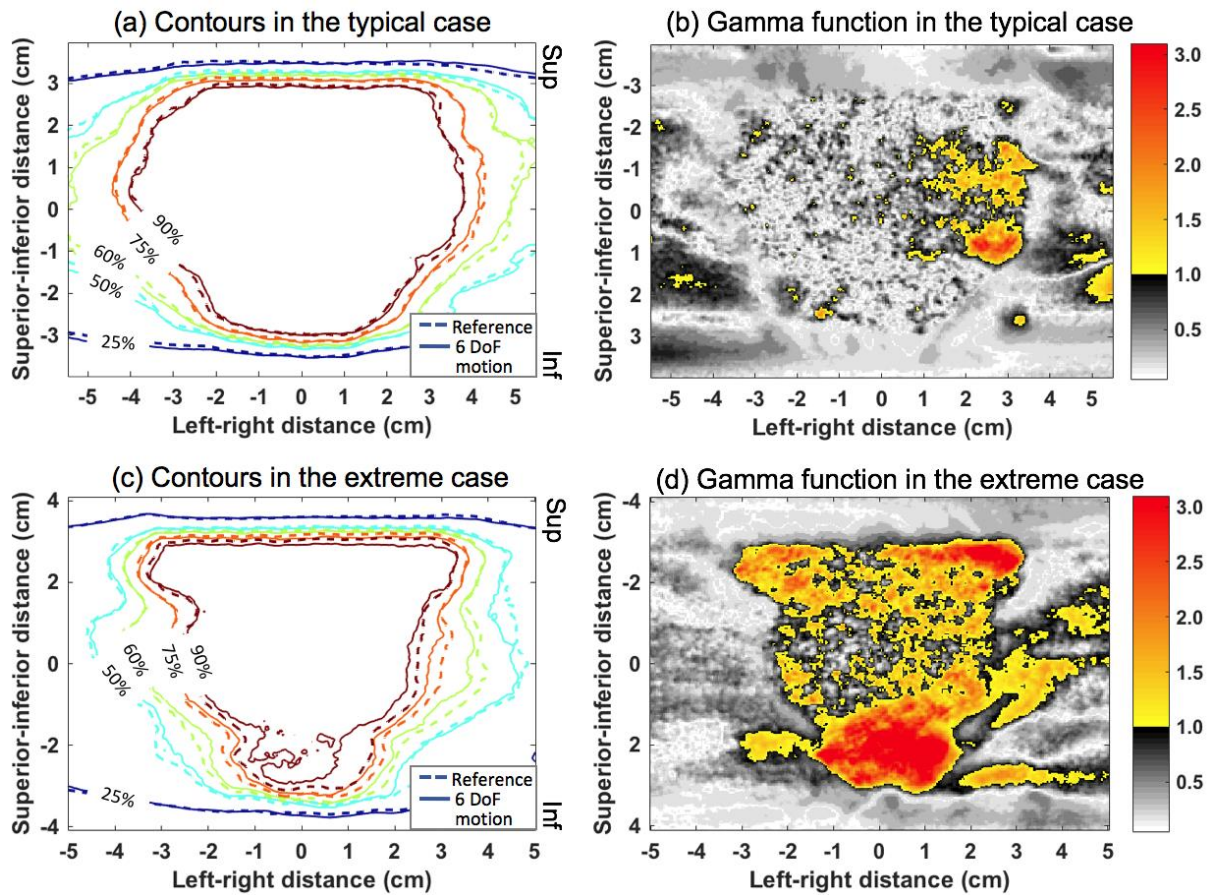
187

188 Figure 7: Gamma pass rate data for a 50% test threshold of the reference dose. Top,
 189 summary of the gamma pass rates for each plan, with a dashed line connecting trace pair
 190 results and the median bar for results from the same trace. Bottom, summary of the
 191 reduction in pass rates caused by rotation.

192

193 The difference in dose contours and gamma function values between the reference film and
 194 the measurement involving 6DoF motion is shown in Figure 8. Two examples using a 90%
 195 test threshold are exhibited, one as a typical case (90.1% pass rate) and the other as an

196 extreme case (35.6% pass rate). In the typical case, the pass rate difference between 6DoF
 197 motion and translation only was 5.4%, while in the extreme case the pass rate
 198 reached 25.8%.



199

200 Figure 8: Dosimetric effects of 6DoF motion in a typical case((a)&(b), 90.1% pass rate) and
 201 an extreme case((c)&(d), 35.6% pass rate). (a)/(c) Dose contours presented as percentage
 202 of the reference dose(1334.0 cGy) for the measurement with 6DoF motion and the reference
 203 film. (b)/(d) Corresponding gamma function values of each pixel in the reference film.

204

205 4. Discussion

206 Film-based dose measurements in a robotically controlled phantom were performed to
207 experimentally investigate whether prostate intrafraction rotation results in influential
208 differences to the delivered dose during treatment. The results showed that a statistically
209 significant dose distribution mismatch beyond the tolerance level of 2%/2 mm could be
210 attributed to intrafraction rotation, degrading target tumor dose coverage and increasing
211 normal tissue exposure. The results are consistent with previous simulation studies reporting
212 decreased CTV/PTV coverage due to prostate rotation.^[6-9]

213 The gamma pass rate reduction due to 6DoF motion on the high dose region (90% max
214 dose) was 5.8% ($\pm 7.1\%$) while the gamma pass rate reduction on medium to high dose
215 region (50% max dose) was 4.1% ($\pm 4.8\%$). We evaluated the gamma failure rate with two
216 different thresholds in order to evaluate the effect of rotational motion outside of the PTV
217 (high dose). To this end, we found the dose error caused by rotation were mainly within the
218 PTV in the plane of measurement, the coronal plane. For rotational motion around the
219 Superior-Inferior and Left-Right axes (roll and tilt) such as the test motion with persistent
220 excursion (Trace 3) and erratic rotation (Trace 4), measurements in the sagittal or axial
221 planes would be better suited to measure the dosimetric error.

222 In the present study, prostate patient plans with different levels of sphericity were included. A
223 regular shaped prostate (plans 3 and 4) that is almost spherical would be less sensitive to
224 rotation than an irregularly shaped prostate such as plan 1 and to a lesser extent, plan 2.
225 Our result indeed showed that plans 3 and 4 were more forgiving than plan 1. These results
226 agree with the modelling study by Wolf et al. (2019).^[20] Increasing the sphericity of the
227 prostate at the contouring stage to ensure a spherical target is potentially a strategy to
228 minimize the effect of unpredictable intrafraction prostate 6DoF motion. However, this
229 strategy can increase the overlap volumes between the PTV and the surrounding organs,
230 which needs careful consideration, especially in the context of SBRT treatments.

231 The results also showed dose failures inside and outside the nominal PTV region. The
232 dependency of dosimetric error on both the motion trace and the geometry of the treatment

233 plan suggests interplay effect between intrafraction 6DoF motion and multi-leaf collimator
234 (MLC) movement during VMAT-based SBRT treatment, as reported by several authors on
235 respiratory motion.^[21-23] Instead of adding extra margins to mitigate the potentially
236 considerable interplay effect,^[24] it could be reduced by measuring motion and correcting for it
237 in real-time. MLC tracking has been experimentally demonstrated to correct translation and
238 in-plane rotation^[25,26] and could be expanded to account for out-of-plane rotation. Similarly,
239 6DoF couches could be used to correct 6DoF target motion, such as a modified HexaPOD
240 couch^[27] where the couch control is linked to the 6DoF target position output. More recently,
241 a parallel kinematics robotic stage was developed for 6DoF head motion compensation
242 during stereotactic radiosurgery.^[28,29] An experiment performed with this robotic stage
243 showed an average increase of 6.8% of the gamma pass rate (1%/1mm criteria) when using
244 6DoF head motion compensation compared with no correction.^[30]

245 Several procedures during the experiment and analysis process may introduce geometric
246 and thus dosimetric uncertainties. The accuracy and precision of Kilovoltage Intrafraction
247 Monitoring algorithm used to obtain the 6 DoF prostate motion trace was $0.2 \pm 1.3^\circ$ and
248 0.1 ± 0.5 mm for rotation and translation.^[31] The robotic arm has a reproducibility of 0.1 mm
249 and 0.2° for translational and rotational motion, respectively. With a triple-channel scanner
250 and recommended film dosimetry protocols the film's measurement accuracy was under 5%
251 and the optical density to dose conversion was accurate to 0.1 cGy.^[32] For image registration
252 quality inside DoseLab, the image's rotational accuracy was controlled below $\pm 0.1^\circ$ using
253 markers drawn on four edges of the film using ImageJ (Version 1.52e, Public domain). The
254 image translational accuracy was within ± 0.7 mm (two pixels) based on dose profiles'
255 comparison. These geometric uncertainties need to be taken into account when interpreting
256 the resulting gamma pass rates of each film and the reproducibility of this study.

257 Although our results point to the likelihood of significant dose degradation effects due to
258 prostate intrafraction rotation, our experimental design had several limitations. The phantom
259 and film holder were not anthropomorphic, thus the radiation transport process would differ

260 from that in the human body. Further, we performed indirect 2D dose distribution
261 comparisons using gamma tests instead of 3D CTV/PTV coverage analysis. To overcome
262 these limitations, future experimental work with anthropomorphic phantoms or polymer gel
263 dosimetry could be conducted.

264 **5. Conclusions**

265 For the first time, the dosimetric impact of intrafraction prostate rotation was evaluated
266 experimentally using clinical **VMAT** prostate treatment plans and patient-measured motion
267 traces executed by a 6DoF robotic arm. The experimental results support the hypothesis that
268 6DoF tumor motion causes significantly larger dose error than translation motion alone.

269 **Acknowledgement**

270 P Keall is funded by an NHMRC Senior Professorial Principal Research Fellowship. D T
271 Nguyen is funded by an NHMRC and a Cancer Institute NSW Early Career Fellowships. This
272 work is supported by a Cancer Australia grant (Priority-driven Collaborative Cancer
273 Research Scheme).

274 Special thanks to the staff at the Royal North Shore Hospital for supporting this work. The
275 authors also thank Dr Helen Ball for providing valuable edits to the manuscript.

276

277 **References**

- 278 1. Aurbry JF, Beaulieu L, Girouard L-M, et al. Measurements of intrafraction motion and
 279 interfraction and intrafraction rotation of prostate by three-dimensional analysis of daily
 280 portal imaging with radiopaque markers. *Int J Radiat Oncol Biol Phys.* 2004;60(1):30-39.
- 281 2. Kupelian P, Willoughby T, Mahadevan A, et al. Multi-institutional clinical experience with the
 282 Calypso system in localization and continuous, real-time monitoring of the prostate gland
 283 during external radiotherapy. *Int J Radiat Oncol Biol Phys.* 2007;67(4):1088-1098.
- 284 3. Deutschmann H, Kametraser G, Steininger P, et al. First clinical release of an online, adaptive,
 285 aperture-based image-guided radiotherapy strategy in intensity-modulated radiotherapy to
 286 correct for inter- and intrafractional rotations of the prostate. *Int J Radiat Oncol Biol Phys.*
 287 2012;83(5):1624-1632.
- 288 4. Kotte ANTJ, Hofman P, Lagendijk JJW, Vulpen Mv, Heide UAvd. Intrafraction motion of the
 289 prostate during external-beam radiation therapy: analysis of 427 patients with implanted
 290 fiducial markers. *Int J Radiat Oncol Biol Phys.* 2007;69(2):419-425.
- 291 5. Noel CE, Santanam L, Olsen JR, Baker KW, Parikh PJ. An automated method for adaptive
 292 radiation therapy for prostate cancer patients using continuous fiducial-based tracking.
 293 *Physics in Medicine and Biology.* 2010;55:65-82.
- 294 6. Amro H, Hamstra D, Mcshan D, et al. The dosimetric impact of prostate rotations during
 295 electromagnetically guided external beam radiation therapy. *Int J Radiat Oncol Biol Phys.*
 296 2013;85(1):230-236.
- 297 7. Tehrani JN, O'Brien RT, Poulsen PR, Keall P. Real-time estimation of prostate tumor rotation
 298 and translation with a kV imaging system based on an iterative closest point algorithm.
 299 *Physics in Medicine and Biology.* 2013;58(23):8517-8533.
- 300 8. Li JS, Jin L, Pollack A, et al. Gains from real-time tracking of prostate motion during external beam
 301 radiation therapy. *Int J Radiat Oncol Biol Phys.* 2009;75(5):1613-1620.
- 302 9. Water Svd, Valli L, Aluwini S, Lanconelli N, Heijmen B, Hoogeman M. Intrafraction prostate
 303 translations and rotations during hypofractionated robotic radiation surgery: dosimetric
 304 impact of correction strategies and margins. *Int J Radiat Oncol Biol Phys.* 2014;88(5):1154-
 305 1160.
- 306 10. Rijkhorst EJ, Lakeman A, Nijkamp J, et al. Strategies for online organ motion correction for
 307 intensity-modulated radiotherapy of prostate cancer: prostate, rectum, and bladder dose
 308 effects. *Int J Radiat Oncol Biol Phys.* 2009;75(4):1254-1260.
- 309 11. Alnaghy S, Kyme A, Caillet V, et al. A six-degree-of-freedom robotic motion system for quality
 310 assurance of real-time image-guided radiotherapy. *Physics in Medicine and Biology.*
 311 2019;64(10).
- 312 12. Keall P, Nguyen DT, O'Brien R, et al. Stereotactic prostate adaptive radiotherapy utilising
 313 kilovoltage intrafraction monitoring: the TROG 15.01 SPARK trial. *BMC Cancer.* 2017;17(180).
- 314 13. Poulsen PR, Cho B, Langen K, Kupelian P, Keall PJ. Three-dimensional prostate position
 315 estimation with a single x-ray imager utilizing the spatial probability density. *Physics in*
 316 *Medicine and Biology.* 2008(53):4331-4353.
- 317 14. Chen Y, Medioni G. Object modeling by registration of multiple range images. *Image and*
 318 *vision computing* 1991;10(3):145-155.
- 319 15. Huang CY, Tehrani JN, Ng JA, Booth J, Keall P. Six degrees-of-freedom prostate and lung tumor
 320 motion measurements using kilovoltage intrafraction monitoring. *Int J Radiat Oncol Biol*
 321 *Phys.* 2015;91(2):368-375.
- 322 16. Keall P, Nguyen DT, O'Brien R, et al. Stereotactic prostate adaptive radiotherapy utilising
 323 kilovoltage intrafraction monitoring: the TROG 15.01 SPARK trial. *BMC Cancer.*
 324 2017;17(180):[Available online].
- 325 17. Pai S, Das IJ, Dempsey JF, et al. TG-69: Radiographic film for megavoltage beam dosimetry.
 326 *medical Physics.* 2007;34(6):2228-2258.

- 327 **18.** Low DA, Harms WB, Mutic S, Purdy JA. A technique for the quantitative evaluation of dose
328 distributions. *Medical Physics*. 1998;25(5):656-661.
- 329 **19.** Ezzell GA, Burmeister JW, Dogan N, et al. IMRT commissioning: Multiple institution planning
330 and dosimetry comparisons, a report from AAPM Task Group 119. *Medical Physics*.
331 2009;36(11):5359-5373.
- 332 **20.** Wolf J, Nicholls J, Hunter P, Nguyen DT, Keall P, Martin J. Dosimetric impact of intrafraction
333 rotations in stereotactic prostate radiotherapy: A subset analysis of the TROG 15.01 SPARK
334 trial. *Radiother Oncol*. July 1 2019;136:143-147.
- 335 **21.** Ong C, Verbakel WFAR, Cuijpers JP, Slotman BJ, Senan S. Dosimetric impact of interplay effect
336 on RapidArc lung stereotactic treatment delivery. *Int. J. Radiat Oncol Biol. Phys*.
337 2011;79(1):305-311.
- 338 **22.** Rao M, Wu J, Cao D, et al. Dosimetric impact of breathing motion in lung stereotactic body
339 radiotherapy treatment using image-modulated radiotherapy and volumetric modulated arc
340 therapy. *Int J Radiat Oncol Biol Phys*. 2012;83(2):e251-e256.
- 341 **23.** Li X, Yang Y, Li T, Fallon K, Heron DE, Huq MS. Dosimetric effect of respiratory motion on
342 volumetric-modulated arc therapy-based lung SBRT treatment delivered by TrueBeam
343 machine with flattening filter-free beam. *Journal of Applied Clinical Medical Physics*.
344 2013;14(6):195-204.
- 345 **24.** Per Rugaard Poulsen MLS, Paul Keall, et al. A method of dose reconstruction for moving
346 targets compatible with dynamic treatments. *Medical Physics*. 2012(39):6237-6246.
- 347 **25.** Keall PJ, Sawant A, Cho B, et al. Electromagnetic-guided dynamic multileaf collimator tracking
348 enables motion management for intensity-modulated arc therapy. *Int. J. Radiat Oncol Biol*.
349 *Phys*. 2011;79(1):312-320.
- 350 **26.** Wu J, Ruan D, Cho B, et al. Electromagnetic detection and real-time DMLC adaption to target
351 rotation during radiotherapy. *Int J Radiat Oncol Biol Phys*. 2012;82(3):e545-e553.
- 352 **27.** Juergen Wilbert KB, Christian Hermann, et al. Accuracy of real-time couch tracking during 3-
353 dimensional conformal radiation therapy, intensity modulated radiation therapy, and
354 volumetric modulated arc therapy for prostate cancer *Int J Radiat Oncol Biol Phys*.
355 2013;85(1):237-242.
- 356 **28.** Belcher A, Liu X, Wiersma RD. Implementing frameless and maskless stereotactic
357 radiosurgery with real-time 6-degrees-of-freedom robotic head motion compensation. *Int J*
358 *Radiat Oncol Biol Phys*. 2016;96(2):e691.
- 359 **29.** Belcher AH, Liu X, Grelewicz Z, Pearson E, Wiersma RD. Development of a 6DoF robotic
360 motion phantom for radiation therapy. *Medical Physics*. 2014;41(12).
- 361 **30.** Belcher A, Farrey K, Liu X, Wiersma R. Evaluation of target dose coverage with real-time
362 robotic head motion stabilization in single-isocenter multi-target SRS: a phantom study: su-e-
363 108-03. *Medical Physics*. 2017;44(6):2725.
- 364 **31.** JH Kim DN, JT Booth, et al. The accuracy and precision of Kilovoltage Intrafraction Monitoring
365 (KIM) six degree-of-freedom prostate motion measurements during patient treatments.
366 *Radiotherapy and Oncology*. 2018;126:236-243.
- 367 **32.** Marroquin EYL, González JAH, López MAC, Barajas JEV, García-Garduño OA. Evaluation of the
368 uncertainty in an EBT3 film dosimetry system utilizing net optical density. *J Appl Clin Med*
369 *Phys*. 2016;17(5):466-481.

370

371 **Footnotes**

- 372 a. UR3 technical details. Universal Robots. [https://www.universal-](https://www.universal-robots.com/media/1801288/eng_199901_ur3_tech_spec_web_a4.pdf)
373 [robots.com/media/1801288/eng_199901_ur3_tech_spec_web_a4.pdf](https://www.universal-robots.com/media/1801288/eng_199901_ur3_tech_spec_web_a4.pdf) Accessed 1st Dec, 2019.

- 374 b. GAFChromic™ EBT3 specification and user guide. Ashland Advanced Materials, 2019.
- 375 http://www.gafchromic.com/documents/EBT3_Specifications.pdf Accessed 1st Dec, 2019.

1 **Experimental evaluation of the dosimetric impact of intrafraction prostate**
2 **rotation using film measurement with a 6DoF robotic arm**

3 Kehuan Shi¹, Andrew Dipuglia², Jeremy Booth², Saree Alnaghy³, Andre Kyme⁴, Paul Keall¹
4 and Doan Trang Nguyen^{1,5}

5 1. ACRF Image-X Institute, Central Clinical School, University of Sydney, Sydney, NSW,
6 Australia

7 2. Northern Sydney Cancer Centre, Royal North Shore Hospital, St Leonards, NSW,
8 Australia

9 3. Centre for Medical Radiation Physics, University of Wollongong, Wollongong, NSW,
10 Australia

11 4. School of Biomedical Engineering, University of Sydney, Sydney, NSW, Australia

12 5. School of Biomedical Engineering, University of Technology Sydney, Sydney, NSW,
13 Australia

14 Correspondence: DoanTrang.Nguyen@uts.edu.au

15